Robust Control of Dual-Linear-Motor-Driven Gantry Stage for Coordinated Contouring Tasks Based on Feed Velocity

Yanbin Liu, Weichao Sun, *Senior Member, IEEE*, Concettina Buccella, *Senior Member, IEEE*, and Carlo Cecati, *Fellow, IEEE*

***Abstract*—Contouring control is one of the most important tasks for the dual-linear-motor-driven gantry system, whose control performance determines the in various precision machining equipment, mainly industrial machine tools. Nevertheless, there are some limitations in present results, including the insufficient consideration of system uncertainty and the approximation errors introduced by the computation of the path length. To overcome these issues, the effects of the rotational dynamic and uncertainties are studied and further refined in this article, and a robust control scheme with adaptive neural network identification is designed based on the desired contouring velocity. The method improves existing approaches and avoids the imperfection of the previous one, based on tracking control under global task coordinate frame. The effects of various environmental forces are considered and the B-spline wavelet neural network is employed to approximate unknown dynamic caused by the thrust ripples of the three motors. Some experiments on a real system verify the effectiveness and superiority of the proposed velocity-based contouring control method**

***Index Terms*—Adaptive control, contouring task, coordinated control, linear motion, neural network.**

NOMENCLATURE

$[\dot{\bullet}, \ddot{\bullet}]$	First and second total derivatives of $\bullet$ w.r.t t.
$[\ell_e, \ell_g, \ell_m]$	Distances between two encoders, parallel guides, and motors, respectively.
$[x_{m_i}]$	Position of the motor Mi measured by the encoder Ei, where $i = 1, 2, 3$. Denote $\bar{x}_m = [x_{m_1}, x_{m_2}, x_{m_3}]^\top$.
$[x]$	Position of the working head along the crossbeam.
$[y]$	Position of the $\tilde{o}$ along Y-axis.
$[\varrho]$	Rotational angle of the crossbeam.
$[q]$	State vector of the system, i.e., $q = [x, y, \varrho]^\top$.
$[h]$	Distance from the centroid point of the working head to $\tilde{o}$ along direction of $\boldsymbol{\beta}$.
$[x_h, y_h]$	Actual position coordinates of the working head under OXY frame.
$[u]$	Vector of the actual input voltage, i.e., $u = [u_1, u_2, u_3]^\top$ where u_i is the actual input voltage of the motor Mi.
$[u_q, u_r]$	Virtual input vectors in inertial coordinate system and task coordinate system, respectively.
$[k_{f_i}]$	Force constant of the motor Mi.
$[f_{mi}]$	Thrust generated by the motor Mi, i.e., $f_{mi} = k_{f_i} u_i$.
$[F_m]$	Thrust vector, i.e., $F_m = [f_{m1}, f_{m2}, f_{m3}]^\top$.
$[T_m]$	Transformation matrix from F_m to u_q.
$[M_x]$	Total load applied to motor M1.
$[M_y]$	Total load applied to motors M2 and M3.
$[J_{\tilde{o}}]$	Sum of rotational inertials of the working head w.r.t C_2 and the crossbeam w.r.t o.
$[A_{f\bullet}, B_\bullet]$	Equivalent coefficients of the Coulomb friction and viscous along $\bullet$-axis.
$[k_\varrho]$	Equivalent stiffness coefficient of the bearings.
$[f_{c_i}(\bullet)]$	Thrust ripple acting on Mi, where $i = 1, 2, 3$.
$[r_c, r_m]$	Coordinates of the working head along the normal and tangential directions of the desired contour.
$[\hat{\bullet}]$	Estimated value of $\bullet$.
$[\tilde{\bullet}]$	Error between $\hat{\bullet}$ and $\bullet$, i.e., $\tilde{\bullet} = \hat{\bullet} - \bullet$.

Manuscript received 22 April 2022; revised 9 July 2022; accepted 4 August 2022. Date of publication 24 August 2022; date of current version 23 January 2023. This work was supported in part by the National Natural Science Foundation of China under Grant U20A20188 and Grant 62022031, in part by the Major Scientific and Technological Research Project of Ningbo under Grant 2021Z040, and in part by the Fundamental Research Funds for the Central Universities. *(Corresponding author: Yanbin Liu.)*

Yanbin Liu and Weichao Sun are with the Research Institute of Intelligent Control and Systems, Harbin Institute of Technology, Harbin 150001, China (e-mail: liu_yb@hit.edu.cn; w.sun@hit.edu.cn).

Concettina Buccella and Carlo Cecati are with the Department of Information Engineering Computer Science and Mathematics, University of L'Aquila and with DigiPower srl, 67100 L'Aquila, Italy (e-mail: concettina.buccella@univaq.it; c.cecati@ieee.org).

Color versions of one or more figures in this article are available at https://doi.org/10.1109/TIE.2022.3199920.

Digital Object Identifier 10.1109/TIE.2022.3199920

I. INTRODUCTION

AS ONE of the core subsystems of many high-end manufacturing equipment, dual-linear-motor-driven gantry system (DLMDGS) has always been a hot topic of study, such as surface mount assembly equipment, photolithography machines, computer numerical control machine tools, optical inspection systems, and so on. With the rapid development of digital and computer technology, the processing and production of traditional industrial products gradually tend to be refined, miniaturized, and high-quality quantification, which demands higher control performance of DLMDGS. In some specific

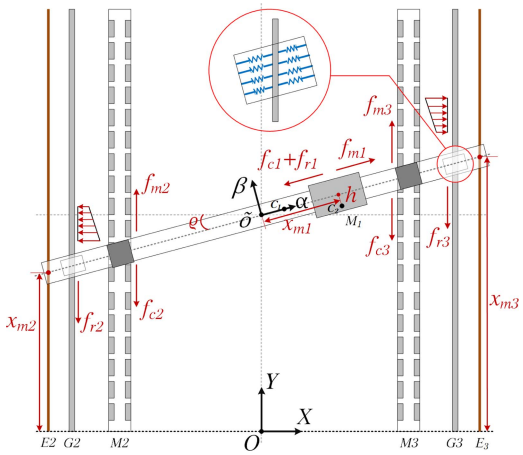

Fig. 1. Schematic diagram of DLMDGS with rotation of the crossbeam.

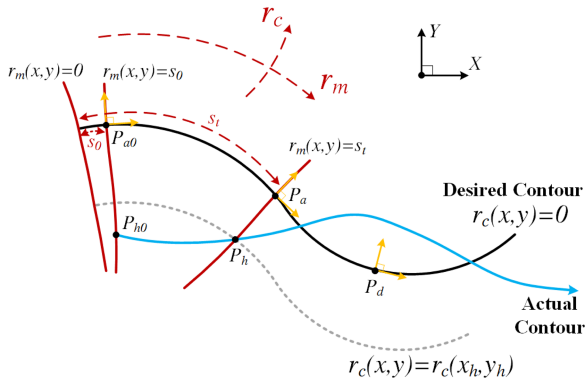

Fig. 2. Orthogonal global task coordinate frame.

production processes, such as 3-D printing, computer numerical control (CNC) drilling machine, CNC milling machine, laser engraving/cutting, etc., the contour accuracy is the core index to evaluate the performance of the equipment [1], [2]. Therefore, it is of great significance to investigate advanced control schemes for the contouring task of DLMDGS to improve their quality and efficiency.

The structure of typical DLMDGSs is shown in Fig. 1, where OXY is the inertial coordinate frame with the horizontal axis $\overrightarrow{OX}$ and the longitudinal axis $\overrightarrow{OY}$, $\tilde{o}$ represents the midpoint of the crossbeam, $\boldsymbol{\alpha}$ and $\boldsymbol{\beta}$ refer to the directions along and perpendicular to the crossbeam, respectively, C_1 and C_2 are the centroid points of the crossbeam and the working head. For such a system, complex nonlinearities and uncertainties of the system are the two main factors which greatly affect the performance of the contouring control and have been investigated extensively, including inertia, friction, thrust ripple, external disturbance, etc. [3], [4], [5], [6]. In recent years, with the development of artificial neural network (ANN), in order to further reduce the impact of nonlinearities and uncertainties on system, many ANN-based control methods have been used to approximate the unknown dynamics and design the controller for linear motor system [7]. In [8], the authors employed radial basis function neural network (RBFNN) to fit the unknown function of the system and designed ARC law to improve the motion precision of the linear motor system. The idea has also been used in the biaxial system. Nevertheless, under these ANN-based control methods, better control effect depends on more neural network hidden layer nodes, and at the same time, it will introduce greater computational burden, which will affect the real-time control performance of the system. Moreover, the structure design of most neural networks is blind due to lacking theoretical basis. In [9], B-spline wavelet neural network was successfully utilized to identify the periodic unknown dynamic of the linear motor driven stage with lower calculation burden, which successfully overcomes the above two problems. Inspired by this, the impact of the complex nonlinearities and uncertainties on contour control performance of DLMDGS could be reduced further.

In addition, the improvements of the coordination performance of the three motors also greatly increase the contouring control precision of the system. For a long time in the past, the coordination control problem of DLMDGS was simplified into two independent problems to be studied separately, i.e., the contouring control problem of planar biaxial system [10], [11], [12], [13], [14], [15], [16] and the synchronous control problem of two motors along the *Y*-axis [17], [18], [19], [20], [21], [22], [23], [24], [26]. In this way, although the contouring control performance can be improved to some extent, the motion coordination of the three linear motors is not fully taken into consideration, and therefore, the improvement is limited. The most impressed research for this topic in recent years is from [27]. Chen et al. [27] effectively investigated the structural characteristics of flexible components and their force coupling along *Y*-axis. Subsequently, a novel three degree-of-freedom (3-DOF) dynamic model was established by directly considering the rotational dynamics of the crossbeam, greatly improving the coordinated control design on the basis of global task coordinate frame (GTCF) approach [27]. For the details, the state of the system is composed of r_c, r_m, and ϱ, where r_c represents the contouring error perpendicular to the direction of the contour; r_m is the distance of movement along the contour; ϱ stands for the rotation angle of the crossbeam. The contouring control problem is transformed into a superposition of the tracking control problem along r_m-axis and stabilization problems along other two axes, which improves the coordination of the three motors. However, there are still some improving potentials. On one hand, the uncertainty of the system, such as thrust ripple has not been fully considered, which makes it possible for the contouring control performance to be further improved. On the other hand, as shown in Fig. 2, $P_h(x_h, y_h)$ is the actual position of the stage at time t; $P_a(x_a, y_a)$ is the closest point on the contour to the point P_h; $P_d(x_d, y_d)$ represents to the desired point on the contour. Under GTCF, the tracking error along the r_m-axis should be calculated in real time for tracking control, i.e., the length of the curve $\widehat{P_aP_d}$ in Fig. 2. In most cases, it is with almost no explicit solution, while numerical methods were often used to approximate it [28], which with the drawback of too much computational burden, moreover they are affected by approximation errors.

This article addresses the problem of the coordination contouring control problems of DLMDGS and designs a robust control scheme with adaptive neural network identification in order to break through the bottleneck of control precision. It is designed based on the desired velocity to avoid the calculation of tracking error along r_m-axis, which spares the calculational cost to improve the performance of contouring control. For the purpose of higher precision of the contouring control, the complex environmental forces are considered and feed-forward compensated by a B-spline wavelet neural network (BSWNN) approximation. Based on the theory of wavelet analysis, the approximation effect of the designed BSWNN is guaranteed, which is also a guiding for the parameter setting of the approximator. A contrast experiment is carried out to validate the efficiency of the proposed control algorithm, where the superiorities of the velocity-field-based control scheme and the designed BSWNN are shown in the results.

The article is organized as follows: In Section II, the modeling and control objective are elaborated in detail. Proposed control scheme is introduced in Section III. The experimental guarantee appears in Section IV. Finally, Section V concludes this article.

II. Modeling and Problem Statement

The concerned control problem is formulated, where the dynamic model of DLMDGS is introduced in Section II-A, and the control objective of the contouring task is shown in Section II-B. In order to simplify the analysis, the independent variables of some functions, function matrices, or function vectors are omitted in subsequent analysis, which does not cause confusion.

A. Dynamic Model of DLMDGS

In general, a DLMDGS is usually arranged in the configuration shown in Fig. 1, in which, one motor located on the crossbeam drives the working head moving along it, and the other two parallel motors fixed on both ends of the crossbeam cooperate to complete the motion tasks along Y-axis. Based on the mechanical analysis in [27], for a real DLMDGS, the rotational dynamics of the crossbeam and the translational movement of the moving stage can be captured by the following Euler–Lagrange dynamic equations:

$$M_q\ddot{q} + C_q\dot{q} + K_\varrho q = T_m F_m - F_e + \delta + d(t) \tag{1}$$

where M_q, C_q, K_ϱ, A_f, and B are the coefficient matrices of inertia, Coriolis/centrifugal force, stiffness, coulomb and viscous; T_m is the transformation matrix from F_m to u_q; their specific forms are shown in (2) shown at the bottom of this page; $\delta = [\delta_1, \delta_2, \delta_3]^\top$ represents the slow time-varying dynamics of the system; $d(t)$ refers to the resulting force of other unknown disturbances and modeling errors; F_e stands for the resultant vector of the environmental forces, mainly including the frictions and thrust ripples, i.e., $F_e = B\dot{q} + A_f S(\dot{q}) + T_m F_c$, where $F_c = [f_{c_1}, f_{c_2}, f_{c_3}]^\top$. Based on the theory of wavelet analysis ([29]), the unknown functions $f_{c_i}(x_{m_i})$ can be fitted by a wavelet series as follows:

$$f_{c_i}(x_{m_i}) = \sum_n W_{i,n}\varphi_{i,n}(x_{m_i}),\ \varphi_{i,n}(\bullet) = \varphi(j_i \bullet - n) \tag{3}$$

where $W_{i,n}$ are the weights of the neuron nodes; $j_i \in \mathbb{Z}$ are the scale parameters; $n \in \mathbb{Z}$ is the translation parameter; $\varphi(\bullet)$ is chosen as a quadratic B-spline mother wavelet ([9]). Subsequently, $F_e = B\dot{q} + A_f S(\dot{q}) + F_{nn}$, where $F_{nn} = \sum_n T_m \Phi_n \overline{W}_n$, $\overline{W}_n = [W_{1,n}, W_{2,n}, W_{3,n}]^\top$, $\Phi_n = \mathrm{Diag}(\varphi_{1,n}(x_{m_1}), \varphi_{2,n}(x_{m_2}), \varphi_{3,n}(x_{m_3}))$.

Denote $\theta = [M_x; M_y; J_{\tilde{o}}; k_\varrho; B_x; B_y; B_\varrho; A_{fx}; A_{fy}; A_{f\varrho}; \delta]$. For the studied system, l_m, l_g, and l_e can be measured easily, and h is approximately zero, due to the almost symmetric structure. Subsequently, the uncertainty parameters and functions of the plant (1) are θ, $\overline{W}_n$, and $d(t)$. For a real DLMDGS, bounds of the unknown parameters and functions can be obtained by preliminary identification ([4], [5], [27]), which implies that the following assumption can be made reasonably.

Assumption 1: There exist known constant vectors $\theta_m = [\theta_{m1}, \ldots, \theta_{m13}]^\top$, $\theta_M = [\theta_{M1}, \ldots, \theta_{M13}]^\top$ and known function vector $\mathcal{F}(q, \dot{q}, t)$ such that

$$\theta_m \le \theta \le \theta_M,\ \ |-T_m F_c + d(t)| \le \mathcal{F}(q, \dot{q}, t).$$

B. Problem Statement

Suppose that the desired contour is $\mathscr{C}(x, y) = 0$, whose parametric equation by arc-length parameterization is $r_d(t) = [x_d(t), y_d(t)]^\top$. The control objective of the contouring task for DLMGDS is to design input laws for u to drive the working head moving along the desired planar contour $r_d(t)$ with feed velocity $\nu_{md}(t) = \sqrt{\dot{x}_d^2(t) + \dot{y}_d^2(t)}$, and meanwhile, ensure the synchronous movement of the two motors in Y-direction. In actual industrial control, $r_d(t)$ is usually a piecewise smooth function with finite angular points, and therefore, the contour task can be divided into several subtasks where the desired contour of each subtask is a smooth function. Without loss of generality, $r_d(t)$ is assumed to be a second-order differentiable function vector.

$$M_q = \begin{bmatrix} M_x & M_x \sin\varrho & M_x h \\ M_x \sin\varrho & M_y & M_x\left(h\sin\varrho + x\cos\varrho\right) \\ M_x h & M_x\left(h\sin\varrho + x\cos\varrho\right) & J_{\tilde{o}} + M_x\left(h^2 + x^2\right) \end{bmatrix},\ T_m = \begin{bmatrix} 1 & 0 & 0 \\ \sin\varrho & 1 & 1 \\ h & -\frac{\ell_m}{2} & \frac{\ell_m}{2} \end{bmatrix}, K_\varrho = \begin{bmatrix} 0 & 0 & 0 \\ 0 & 0 & 0 \\ 0 & 0 & k_\varrho \end{bmatrix},$$

$$C_q = \begin{bmatrix} 0 & 0 & -M_x x\dot{\varrho} \\ M_x\dot{\varrho}\cos\varrho & 0 & M_x\left[(h\dot{\varrho} + \dot{x})\cos\varrho - x\dot{\varrho}\sin\varrho\right] \\ M_x x\dot{\varrho} & 0 & M_x x\dot{x} \end{bmatrix}, B = \begin{bmatrix} B_x & 0 & 0 \\ B_x\sin\varrho & B_y & B_{\tilde{o}}\frac{\ell_g}{2} \\ hB_x & B_{\tilde{o}}\frac{\ell_g}{2} & B_y\frac{\ell_g^2}{4} \end{bmatrix}, A_f = \begin{bmatrix} A_{fx} & 0 & 0 \\ A_{fx}\sin\varrho & A_{fy} & 0 \\ hA_{fx} & A_{f\tilde{o}}\frac{\ell_g}{2} & 0 \end{bmatrix}. \tag{2}$$

Under GTCF ([16], [27]), the state of DLMDGS is $q_r = [r_c, r_m, \varrho]^\top$, where the Jacobi matrix from q to q_r is

$$J = \begin{bmatrix} \frac{\mathscr{C}_x}{\sqrt{\mathscr{C}_x^2+\mathscr{C}_y^2}} & \frac{\mathscr{C}_y}{\sqrt{\mathscr{C}_x^2+\mathscr{C}_y^2}} & 0 \\ \frac{-\mathscr{C}_y}{\sqrt{\mathscr{C}_x^2+\mathscr{C}_y^2}} & \frac{\mathscr{C}_x}{\sqrt{\mathscr{C}_x^2+\mathscr{C}_y^2}} & 0 \\ 0 & 0 & 1 \end{bmatrix} \begin{bmatrix} \cos\varrho & 0 & -x\sin\varrho \\ \sin\varrho & 1 & x\cos\varrho \\ 0 & 0 & 1 \end{bmatrix},$$

in which $\mathscr{C}_x$ and $\mathscr{C}_y$ are the partial derivatives of $\mathscr{C}$ w.r.t x and y, respectively. Thus,

$$\dot{q}_r = J\dot{q}. \tag{4}$$

It should be noted that for an actual system, the rotation angle of the crossbeam is very small, so that J is invertible. Subsequently, in the task space, the dynamic model of the system can be rewritten as follows:

$$M_r\ddot{q}_r + C_r\dot{q}_r + K_r q_r = T_{mr}F_m - F_{er} + \delta_r + d_r \tag{5}$$

where $M_r = J^{-\top}M_qJ^{-1}$, $C_r = J^{-\top}(C_q - M_qJ^{-1}\dot{J})J^{-1}$, $K_r = J^{-\top}K_\varrho J^{-1}$, $T_{mr} = J^{-\top}T_m$, $F_{er} = J^{-\top}F_e$, $\delta_r = J^{-\top}\delta$, and $d_r = J^{-\top}d$. It should be noted that a real DLMDGS is always assumed to be a rigid body with the finite load, and thus, from the definitions of M_r, C_r, and K_r, the following properties hold for DLMDGS.

Property 1: In any finite work space, M_r is a symmetric positive definite matrix satisfying $\zeta_1 I \le M_r \le \zeta_2 I$, with ζ_1 and ζ_q being positive scalars.

Property 2: $\dot{M}_r - 2C_r$ is skew-symmetric.

Property 3: M_r, C_r, and K_r can be linearly parameterized by M_x, M_y, $J_{\tilde{o}}$, and K_ϱ.

As mentioned, r_m is almost with nonexistent explicit solution. To avoid calculating r_m, a control approach without the feedback of r_m is required to avoid the above issue. For a contouring task, the working head are expected to be stabilized at zero along r_c- and ϱ-axes and to move with desired feed speed $\nu_{md}(t)$ along r_m-axis, which implies that the tracking performance along r_m-axis is not critical. Therefore, the control objective for the contouring task of DLMDGS can be described in the task space as follows.

Control objective: For a known desired contour $r_d(t)$ with the shape function $\mathscr{C}$ and feed velocity $\nu_{md}(t)$, design law for u such that r_c, ϱ and $\dot{r}_m - \nu_{md}$ are as small as possible in spite of the complex uncertainties of the system.

III. Main Results

In this section, an adaptive neural network control law for u is designed to achieve the control objective. First, the following definition is necessary for the subsequent analysis:

$$\sigma(r_c, \varrho, \dot{q}_r, t) = \dot{q}_r - \nu_d \tag{6}$$

where $\nu_d = [-k_c r_c, \nu_{md}(t), -k_\varrho\varrho]^\top$; k_c and k_ϱ are two positive constants. Then, from (5) and (6), σ satisfies

$$M_r\dot{\sigma} + C_r\sigma = T_{mr}F_m - J^{-\top}F_\theta - F_{\text{nnr}} + d_r \tag{7}$$

where $F_\theta = B\dot{q} + A_f S(\dot{q}) + T_m F_c + J^\top C_r\nu_d + K_\varrho q + \delta + J^\top M_r\dot{\nu}_d$. From Property 3, F_θ can be linearly parameterized by θ, i.e., $F_\theta = \Phi_\theta(q, \dot{q}, t)\theta$.

Subsequently, the robust control law for u is designed, whose structure is shown in Fig. 3

$$\begin{aligned} u &= T_c^{-1}\left(J^\top u_s + u_a + u_{nn} + u_z\right),\ u_a = \Phi_\theta\left(q, \dot{q}, t\right)\hat{\theta} \\ T_c &= T_m\text{Diag}\left(k_{m_1}, k_{m_2}, k_{m_3}\right),\ u_{nn} = \mathcal{B}\left(\hat{F}_{nn}, \mathcal{F}\right) \\ u_s &= u_{s1} + u_{s2},\ u_{s1} = -K_\sigma\sigma - K_0 q_r \\ u_z &= -K_z z,\ z = q - [x_d, y_d, 0]^\top \end{aligned} \tag{8}$$

where u_a and u_{nn} refer to the feed-forward term to compensate the unknown forces F_θ and F_{nnr}, respectively; u_z is the position feedback term to avoid the position deviation; $K_z > 0$; u_{s1} and u_{s2} represent the terms of the state feedback compensation and robust feedback compensation, respectively; $K_\sigma > 0$; $K_0 = \text{Diag}(1, 0, 1)$; $\mathcal{B}(\hat{F}_{nn}, \mathcal{F})$ is a vector valued function, whose ith component is defined as $\mathcal{B}_i = \eta_i\mathcal{S}(\hat{F}_{nni}/\mathcal{F}_i)$, $i = 1, 2, 3$; $\hat{F}_{nni}$ and $\mathcal{F}_i$ are the ith component of $\hat{F}_{nn}$ and $\mathcal{F}$ respectively; $\mathcal{S}(\bullet)$ represents the saturation function; the weights $\hat{\overline{W}}_n$ and parameter estimation $\hat{\theta}$ are updated by

$$\dot{\hat{\overline{W}}}_n = \mathcal{P}_w(\Upsilon_{w,n}\tau_{w,n}), \quad \dot{\hat{\theta}} = \mathcal{P}_\theta(\Upsilon_\theta\tau_\theta) \tag{9}$$

in which $0 < \Upsilon_{w,n} \in \mathbb{R}^{3\times3}$ and $0 < \Upsilon_\theta \in \mathbb{R}^{13\times13}$ are the step matrices of the updating laws; $\tau_{w,n}$ and τ_θ are the updating laws for $\hat{\overline{W}}_n$ and $\hat{\theta}$; $\mathcal{P}_w(\bullet) : \mathbb{R}^3 \to \mathbb{R}^3$ and $\mathcal{P}_\theta(\bullet) : \mathbb{R}^{13} \to \mathbb{R}^{13}$ are two projection mappings, whose ith element is defined as follows:

$$\mathcal{P}_{wi}(\bullet_i) = \begin{cases} 0, & \text{if } \hat{F}_{nn} \ge \mathcal{F} \text{ and } \bullet_i > 0 \\ 0, & \text{if } \hat{F}_{nn} \le -\mathcal{F} \text{ and } \bullet_i < 0 \\ \bullet_i, & \text{otherwise} \end{cases}$$

$$\mathcal{P}_{\theta i}(\bullet_i) = \begin{cases} 0, & \text{if } \hat{\theta} \ge \theta_{iM} \text{ and } \bullet_i > 0 \\ 0, & \text{if } \hat{\theta} \le \theta_{im} \text{ and } \bullet_i < 0 \\ \bullet_i, & \text{otherwise.} \end{cases} \tag{10}$$

According to (9) and (10), it can be obtainted that if $\hat{\theta}(0) \in [\theta_m, \theta_M]$ and $|u_{nn}(0)| \le \mathcal{F}(q, \dot{q}, t)$, then for all $t \ge 0$

$$\hat{\theta}(t) \in [\theta_m, \theta_M], \quad |\hat{F}_{nn}(t)| \le \mathcal{F}(q, \dot{q}, t). \tag{11}$$

Then, the robust law u_{s2} is designed satisfying

$$\sigma^\top u_{s2} \le 0, \quad \sigma^\top\left(u_{s2} + \bar{F}_{\text{nnr}} + \bar{F}_\theta + d_r\right) \le \varepsilon \tag{12}$$

where $\bar{F}_{\text{nnr}} = J^{-\top}u_{nn} - F_{\text{nnr}}$; $\bar{F}_\theta = u_a - F_\theta$; $\varepsilon > 0$ is a constant. An example for u_{s2} is shown as follows:

$$u_{s2} = -H(q, \dot{q}, t)\tanh\left(\frac{\sigma^\top H(q, \dot{q}, t)}{\varepsilon}\right) \tag{13}$$

in which $H(q_r, \dot{q}_r, t)$ is a known function satisfying

$$H(q_r, \dot{q}_r, t) \ge \left\|J^{-\top}\right\|\left(2\mathcal{F} + |\Phi_\theta(\theta_M - \theta_m)|\right). \tag{14}$$

The stability of the closed-loop system consisting of the plant (5) and the control law (8)–(14) is illustrated in the following theorem.

Theorem 1: For any system with the dynamic model (1), if the Assumption 1 and Properties 1 to 3 hold, then, in any finite work space and feed velocity, the concerned system is ultimately

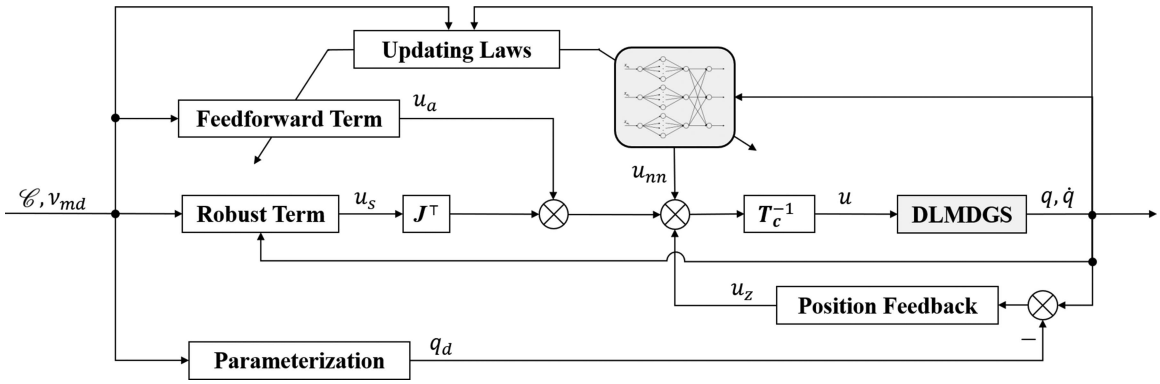

Fig. 3. Block diagram of the closed-loop system under the designed control scheme.

uniformly bounded (UUB) under the control scheme (8)–(14) with arbitrary updating laws τ_θ and $\tau_{w,n}$.

The following lemma is required to prove Theorem 1.

Lemma 1: Consider the following two systems:

$$\text{(I) } \dot{x} = f(x,t), \quad \text{(II) } \dot{x} = f(x,t) - Kx \tag{15}$$

where $x \in \mathbb{R}^i$; $i \in \mathbb{Z}^+$; $f : \mathbb{R}^i \times \mathbb{R} \to \mathbb{R}^i$; $K \in \mathbb{R}^{i\times i}$ is any positive definite matrix. Denote $x_1(t;t_0,x_0)$ and $x_2(t;t_0,x_0)$ are the solutions of the system (I) and (II) with the initial state $x_1(t_0) = x_2(t_0) = x_0$, respectively. Then

$$|x_2(t;t_0,x_0)| \le |x_1(t;t_0,x_0)| \ \ \forall t \ge t_0. \tag{16}$$

Proof: Consider the derivative of $V(x) = x^\top x$ for (I) and (II)

$$\text{(I) } \dot{V} = 2x^\top f(x,t), \quad \text{(II) } \dot{V} = 2x^\top f(x,t) - 2x^\top Kx. \tag{17}$$

Noting that $K > 0$ and invoking the comparison theorem ([30]), Lemma 1 holds. ■

Proof of Theorem 1: Consider the system (1) under the following control law:

$$u = T_c^{-1}(J^\top u_s + u_a + u_{nn}) \tag{18}$$

where u_s, u_a, and u_{nn} are the same as those in (8). Consider the following positive definite function:

$$V_s(q,\dot{q}_r,t) = \frac{1}{2}r_c^2 + \frac{1}{2}\varrho^2 + \frac{1}{2}\sigma^\top M_r \sigma. \tag{19}$$

Invoking Property 2, (7), (12), and (18), the derivative of V_s satisfies

$$\dot{V}_s \le -k_c r_c^2 - k_\varrho \varrho^2 - K_\sigma \sigma^\top \sigma + \varepsilon \le -k_{\min} V_s + \varepsilon \tag{20}$$

where $k_{\min} = \min\{k_c, k_\varrho, \lambda_m(K_\sigma)/\zeta_2\}$; $\lambda_m(K_\sigma)$ is the minimum eigenvalue of K_σ. From comparison theorem ([30])

$$V_s \le -e^{-2k_{\min}t}V_{s0} + \frac{\varepsilon}{2k_{\min}}\left(1 - e^{-2k_{\min}t}\right) \tag{21}$$

where V_{s0} is the initial value of V_s. Noting that $e^{-2k_{\min}t}$ converges to 0 as the time goes on, therefore, it can be obtained that $\lim_{t\to\infty} V_s \le \varepsilon/(2k_{\min})$, which implies that the closed-loop system consisting of (1) and (18) is UUB. Comparing the control laws (8) and (18), and according to Lemma 1, Theorem 1 holds. ■

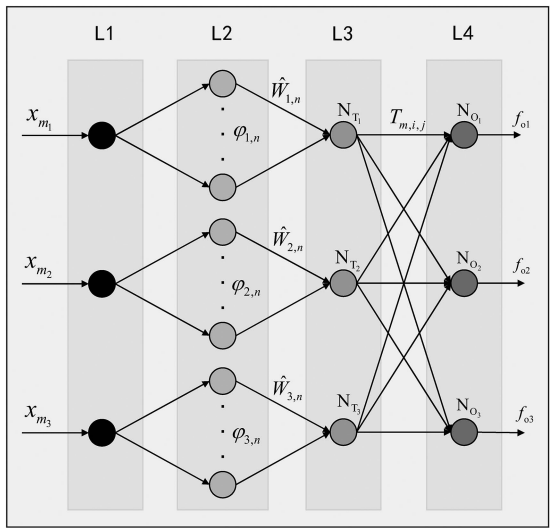

Fig. 4. Structure diagram of the designed B-spline wavelet neural network.

Remark 1: Actually, u_{nn} is in the form of neural network with four layer, as shown in Fig. 4, where the details are given as follows.

- L1: The first layer is the input layer with three nodes whose inputs are x_{m_1}, x_{m_2}, and x_{m_3}, respectively. The activation function for the node with the input x_{m_i} is $\psi_{1,i}(\bullet) = j_i \bullet$.
- L2: The second layer is the wavelet layer. There are three types of neuron nodes in this layer, whose inputs are $j_1 x_{m_1}$, $j_2 x_{m_2}$, and $j_3 x_{m_3}$, respectively. The number of neuron nodes is determined by the travel lengths of three motors and the compact support of the mother wavelet. The activation function for each node is $\psi_{2,i,n}(\bullet) = \varphi(\bullet - n)$, where the subscript i, n refers to the nth node with the input $j_i x_{m_i}$. The connection weight between the input and wavelet layers is constant and defaults to 1.
- L3: The third layer is the transition layer. There are three nodes: N_{T_1}, N_{T_2}, and N_{T_3}. The node N_{T_i} is connected to those with the activation function $\psi_{2,i,n}$ in the wavelet layer, whose connection weight is $\hat{W}_{i,n}$. The activation function for all nodes is $\psi_{3,i}(\bullet) = \bullet, i = 1,2,3$.

L4: The fourth layer is the output layer. There are three nodes which are fully connected with the nodes in transition layer with the weights $T_{m,\imath,\jmath}$. $T_{m,\imath,\jmath}$ represents the element on $\imath$ row, $\jmath$ column of the matrix T_m. The activation functions are $\psi_{4,i} = \mathcal{B}_i(\bullet, \mathcal{F}_i)$.

Remark 2: In theory, the control scheme (18) can also achieve good control performance. However, in actual contouring control task, it may happen that the stage only tracks part of the desired contour, especially at the end of the desired trajectory, due to the lack of compensation for tracking error along r_m- axis. In addition, the position deviation along r_m- axis also seriously affects the performance of the contouring error by reason of the coupling between the motions along $X-$ and $Y-$ axes. Therefore, u_z is designed to compensate for the position deviation along the curve to overcome these problems.

Theorem 2: If there is only parametric uncertainty in the system after a while, i.e., there exists $t_a > 0$ such that $d(t) = 0$ for all $t \geq t_a \geq 0$, the closed-loop system is asymptotically stable under the control scheme (8) and the following updating laws:

$$\tau_\theta = -\Phi_\theta \sigma, \quad \tau_{w,n} = -T_m^\top \Phi_{w,n}^\top T_m^\top J^{-1} \sigma. \tag{22}$$

Proof: According to Lemma 1, it is only needed to prove that the closed-loop system is asymptotically stable under the control scheme (18).

Consider the following positive definite function:

$$V_a(q, \dot{q}_r, t) = V_s + \frac{1}{2}\tilde{\theta}^\top \Upsilon_\theta^{-1} + \frac{1}{2}\sum_n \tilde{\overline{W}}_n^\top \Upsilon_{w,n}^{-1} \tilde{\overline{W}}_n. \tag{23}$$

Taking the derivative of V_a, it becomes

$$\begin{aligned} \dot{V}_a = & -k_c r_c^2 - k_\varrho \varrho^2 + \sigma^\top K_0 q_r \\ & + \sigma^\top \left(J^{-\top} T_c u - F_\theta - F_{\text{nnr}} \right) \\ & + \tilde{\theta}^\top \Upsilon_\theta^{-1} \dot{\hat{\theta}} + \sum_n \tilde{\overline{W}}_n^\top \Upsilon_{w,n}^{-1} \dot{\hat{\overline{W}}}_n. \end{aligned} \tag{24}$$

Substituting the control law (18) and the updating laws (22) into (24), $\dot{V}_a$ satisfies

$$\begin{aligned} \dot{V}_a \leq & -k_c r_c^2 - k_\varrho \varrho^2 - K_\sigma \sigma^\top \sigma + \sigma^\top \left(\bar{F}_{\text{nnr}} + \bar{F}_\theta \right) \\ & + \tilde{\theta}^\top \Upsilon_\theta^{-1} \dot{\hat{\theta}} + \sum_n \tilde{\overline{W}}_n^\top \Upsilon_{w,n}^{-1} \dot{\hat{\overline{W}}}_n \\ \leq & -k_c r_c^2 - k_\varrho \varrho^2 - K_\sigma \sigma^\top \sigma + \tilde{\theta}^\top \Upsilon_\theta^{-1} \dot{\hat{\theta}} \\ & + \tilde{\theta}^\top \Phi_\theta^\top \sigma + \bar{F}_{\text{nnr}}^\top \sigma + \sum_n \tilde{\overline{W}}_n^\top \Upsilon_{w,n}^{-1} \dot{\hat{\overline{W}}}_n \\ \leq & -k_c r_c^2 - k_\varrho \varrho^2 - K_\sigma \sigma^\top \sigma \\ & + \tilde{\theta}^\top \Upsilon_\theta^{-1} \mathcal{P}_\theta(\Upsilon_\theta \tau_\theta) + \tilde{\theta}^\top \Phi_\theta^\top \sigma \\ & + \bar{F}_{\text{nnr}}^\top \sigma + \sum_n \tilde{\overline{W}}_n^\top \Upsilon_{w,n}^{-1} \mathcal{P}_w(\Upsilon_{w,n} \tau_{w,n}). \end{aligned} \tag{25}$$

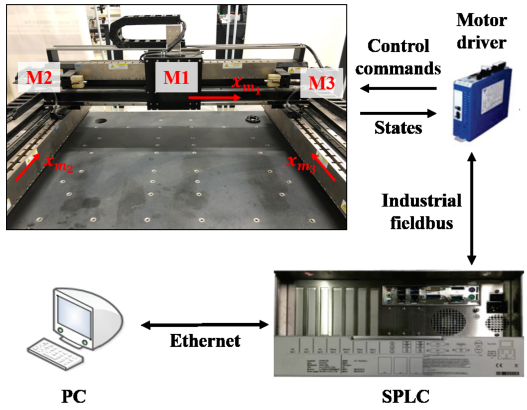

Fig. 5. Experimental equipment of the dual-linear-motor-driven gantry stage.

Based on (10) and (22), it is obvious that

$$\begin{cases} \tilde{\theta}^\top \Upsilon_\theta^{-1} \mathcal{P}_\theta(\Upsilon_\theta \tau_\theta) + \tilde{\theta}^\top \Phi_\theta^\top \sigma \leq 0 \\ \bar{F}_{\text{nnr}}^\top \sigma + \sum_n \tilde{\overline{W}}_n^\top \Upsilon_{w,n}^{-1} \mathcal{P}_w(\Upsilon_{w,n} \tau_{w,n}) \leq 0. \end{cases} \tag{26}$$

Subsequently, (30) becomes

$$\dot{V}_a \leq -k_c r_c^2 - k_\varrho \varrho^2 - K_\sigma \sigma^\top \sigma \tag{27}$$

which implies that the system is asymptotically stable under the control law (18). ■

Remark 3: For a real system, it is a tough assumption that there is only parametric uncertainty in the system. However, it is of great significance to the theoretical research on high precision control of linear motor. The results show that arbitrary control precision can be achieved for the closed-loop system as long as the structure of the dynamic model is accurate enough, even though there are unknown paramters in the system. Therefore, the high precision control problem is transformed into how to approximate the unknown function in the model with high accuracy.

IV. Experimental Results

A. Experiment and Environment Setup

To validate the effectiveness of the proposed control structure and the designed B-spline wavelet neural network, tests of four control approaches were carried out on a real DLMDGS shown in Fig. 5. The control input voltages are calculated by programming at TwinCAT3.0 in real-time patched Microsoft Windows OS, after which the SPLC, as the motion controller, works out the real-time driving current commands for each motor driver to drive the moving platform. The maximal travel lengths of the *X*- and *Y*-axis are 700 and 650 mm, respectively. Each motor is equipped with a grating linear displacement sensor with the accuracy of 50 nm to measure the displacement. After preidentification of the equipment, the nominal parameter values and their ranges of the equipment can be obtained, where the details are listed in Table I. In addition, it should be emphasized that for an actual DLMDGS, the rotational angle of the crossbeam is pretty small, and therefore, it is reasonable that $\cos\varrho \approx 1$, $\sin\varrho \approx \varrho$.

TABLE I
PARAMETERS OF THE EXPERIMENTAL DLMDGS

	Parameter	Nominal Value	Range
X-axis	M_x	11 kg	[8,15] kg
	B_x	26 kg/s	[15,35] kg/s
	A_{fx}	4.1 N	[2,8] N
	δ_1	0 N	[-100,100] N
Y-axis	M_y	37 kg	[30,50] kg
	B_y	8 kg/s	[2,20] kg/s
	A_{fy}	3.6 N	[2,8] N
	δ_2	0 N	[-100,100] N
ϱ-axis	J_M	58 kgÂ·m^2	[45,70] kgÂ·m^2
	B_c	28.7 kg/s	[-50,50] kg/s
	A_{fc}	4.5 N	[-8,8] N
	k_ϱ	2.2×10^6 N	[0.5,4]$\times 10^6$ N
	δ_3	0 NÂ·m	[-100,100] NÂ·m

The details and parameter settings of the four control schemes are listed as follows.

C1: (PID) The proportional-integral-derivative (PID) control law in the following form was employed to drive the system:

$$u = T_c^{-1} J^\top \left(-K_p e_r - K_d \dot{e}_r - K_i \int_0^t e_r(t)\mathrm{d}t \right) \tag{28}$$

where $K_p, K_d, K_i > 0; e_r = q_r - q_{rd}; q_{rd} = [0, s_t, 0]^\top$ was the desired value of q_r; s_t was approximate by the method in [16]. The parameters were set as $K_p = \mathrm{Diag}(3000, 2000, 4000)$, $K_d = \mathrm{Diag}(25, 20, 15)$, and $K_i = \mathrm{Diag}(5000, 2000, 40000)$.

C2: (ARC) The adaptive robust control approach proposed in [27] was tested on the equipment, which consists of feed-forward term to compensate the nonlinear dynamics and robust feedback term to ensure the stability of the system. The parameters of the robust term were set as $\Lambda_r = \mathrm{Diag}(120, 100, 270)$, $K_{s1} = \mathrm{Diag}(25, 20, 15)$, $K_{re} = (500, 500, 500)$, and $K_{ra} = (500, 500, 500)$. The parameters of the recursive least square method were set as $\mu = 0.02$, $\kappa = 0.1$, and $\rho_M = 5000$. The initial value of Γ_l was set as $\Gamma_l(0) = I_{13\times 13}$.

C3: (Proposed method without the neural network) The control approach (8) without the designed B-spline wavelet neural network was applied to drive the three motors, where the parameter estimation $\hat{\theta}$ was updated by the law in (9). The parameter settings of the control law and updating law were given as follows. $k_c = 5000$, $k_\varrho = 4000$, $K_\sigma = \mathrm{Diag}(25, 20, 15)$, $K_z = \mathrm{Diag}(500, 500, 500)$, $\varepsilon = 10$, $\Upsilon_\theta = \mathrm{Diag}(0.01, 10, 10, 1000, 0.01, 10, 10, 1000, 1, 10, 10, 100, 1000)$.

C4: (Proposed method) Drive the equipment under the control scheme (8) with adaptive laws (9). The B-spline mother wavelet was chosen as

$$\varphi(\bullet) = \begin{cases} 2(\bullet + 1)^2, & -1 \le \bullet \le 0 \\ 3 - 4\left(\bullet - \frac{1}{2}\right)^2, & 0 \le \bullet \le 1 \\ 2(\bullet - 2)^2, & 1 \le \bullet \le 2 \\ 0, & \text{otherwise.} \end{cases} \tag{29}$$

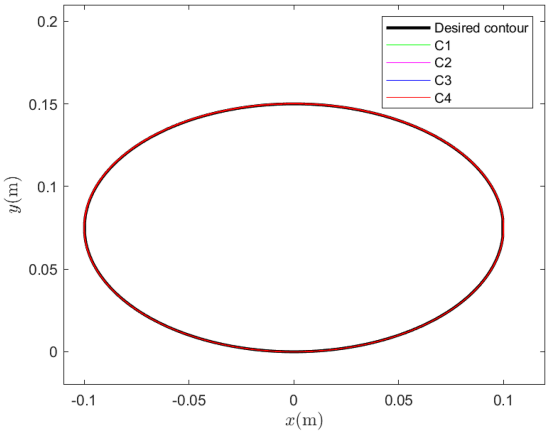

Fig. 6. Motion paths of the working head under the four control schemes.

The scale parameter was set as $j_1 = j_2 = j_3 = 100$. The step parameter of the weight updating was set as $\Upsilon_{w,n} = \mathrm{Diag}(0.02, 0.02, 0.02)$. In addition, other parameters of the control law and updating law were set as the same as C3.

Actually, the above settings ensure that the corresponding coefficients of the state feedback are the same under the three methods. All testings are completed in the same surroundings so that ensure the fairness of the contrast experiment, and the control intervals of them are fixed as 0.25 ms. The desired contour is an ellipse with the major axis of $a = 0.1$ m and the minor axis of $b = 0.075$ m, i.e., the shape function of the desired contour is

$$\frac{x^2}{a^2} + \frac{y^2}{b^2} = 1. \tag{30}$$

The feed angular velocity is set as $\omega = 4$ rad/s, on which the desired trajectories for X- and Y- axes are defined as

$$\begin{cases} x_d(t) = 0.1 \sin(\omega t) \text{ m} \\ y_d(t) = 0.075\,(1 - \cos(\omega t)) \text{ m}. \end{cases} \tag{31}$$

For smooth startup of the equipment, the actual feed angular velocity is set to start at 0 rad/s and gradually increase to 4 rad/s over time, i.e., $\omega = 4(1 - e^{-t})$ rad/s. The concerned testing segment is the last 10 s of the testing, where the feed angular velocity is 4 rad/s and the performance of the system goes to steady state.

B. Experimental Results and Discussions

Figs. 6 to 8 plot the graph of the motion paths, contouring errors, and crossbeam rotation angles of the system under the considered three control approaches. Although Fig. 6 shows that the working head of the equipment moves along the desired contour with high precision under all four control methods, there are still some differences in performance for the differences of the feed-forward compensation for system nonlinearity.

Under the control approach C1, the contouring error and rotation angle of the system were restrained by the proportional, integral, and differential linear feedback of the errors without any compensation for the nonlinear dynamics of the system.

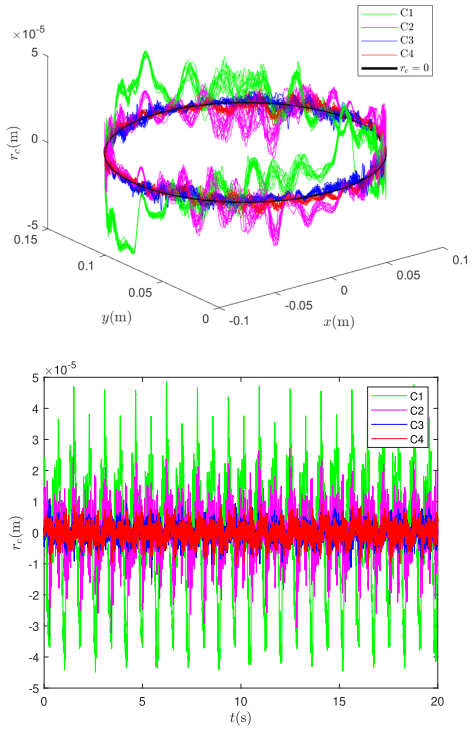

Fig. 7. Contouring errors of the system under the four control schemes.

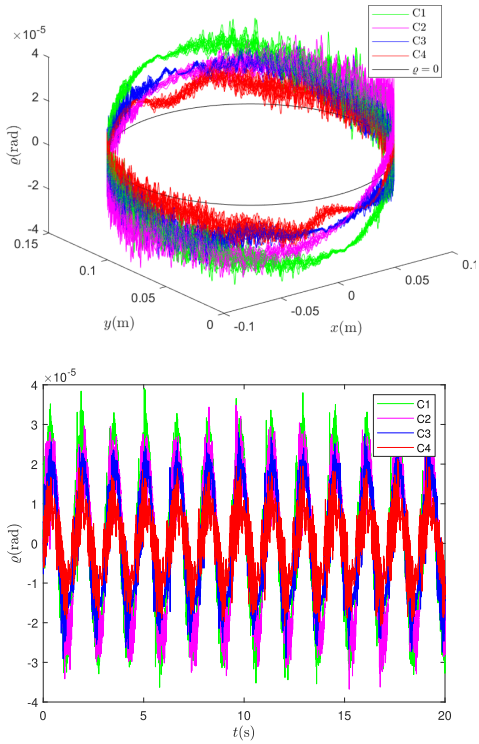

Fig. 8. Rotation angles of the crossbeam under the four control schemes.

Consequently, the results were unsatisfactory both on the precision of the contouring control and the motion coordination of three motors. Compared with C1, the method C2 further compensates for the friction forces feed-forward according to the parameters identified through the recursive least squares method, under which the precision of the contouring error is enhanced considerably compared with C1. Nonetheless, the estimation of the tracking error along r_m-axis was required for both the two approaches, which introduced errors in numerical calculation to affect the contouring performance.

Compared with the results under the method C2, the approach C3 considered the velocity feedback along r_m-axis, where the position compensation was carried out by the PID feedback of the tracking errors of three motors. Since the calculation of the tracking error along r_m-axis was avoided under C3, the contouring precision was improved further, which was validated by the experimental results shown in Fig. 7. Therefore, the structure of the C3 control approach is effective in improving the coordination of the motion of three motors. However, as shown in Fig. 8, due to the lack of compensation for the thrust ripples of three motors, the results of the synchronization control under the three methods were unsatisfactory.

For the controlled equipment, the frictions caused by the guides G2 and G3 are virtually the same, while the rotation of the crossbeam is predominantly caused by thrust ripples of the motors M2 and M3. Under the proposed method, the thrust ripples of three motors were compensated by the designed B-spline wavelet neural network. Hence, the synchronization of the motion of the motors M2 and M3 was significantly enhanced, which is validated by the results shown in Fig. 8.

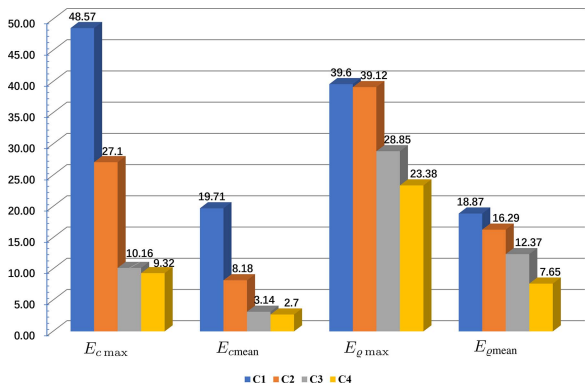

Fig. 9. Indexes of the four testings (μm).

Fig. 9 displays the maximum value and root-mean-square value of r_c and ϱ over the concerned testing segment, where the four indexes are defined as follows.

1) The maximum value of the contouring error over the concerned testing segment:

$$E_{c\max} = \max_t \{r_c(t)\}.$$

2) The root-mean-square value of the contouring error over the concerned testing segment:

$$E_{c\text{mean}} = \left(\frac{1}{N_\tau}\sum_{i=0}^{N_\tau} r_c^2(t_0 + i\tau)\right)^{\frac{1}{2}}$$

where N_τ is the number of sampling over the concerned testing segment; t_0 represents the initial time of the concerned testing segment.

3) The maximum value of the rotation angle over the concerned testing segment

$$E_{\varrho\max} = \max_t \{\varrho(t)\}.$$

4) The root-mean-square value of the rotation angle over the concerned testing segment

$$E_{\varrho\text{mean}} = \left(\frac{1}{N_\tau}\sum_{i=0}^{N_\tau}\varrho^2(t_0+i\tau)\right)^{\frac{1}{2}}.$$

From the results, compared with the control algorithm proposed in [27], the contouring control precision of the system under the proposed velocity-based control algorithm was improved at least 62.51% and 61.61% for the maximum value and the root-mean-square value. In addition, with the designed B-spline wavelet neural work, the values of $E_{\varrho\max}$ and $E_{\varrho\text{mean}}$ are reduced more than 18.96% and 38.16% compared with the method without neural network.

V. Conclusion

An adaptive neural networks control scheme was proposed for coordinate contouring tasks based on the feed velocity. On the basis of stability, the proposed method ensures the performances of both the contouring control and synchronization control. Under the proposed control law, only the velocity along the desired contour is required instead of the arc length, which avoids the calculation of the state r_m. Therefore, it avoids the numerical approximation error and saves the calculation cost. For the complex uncertainties of the system, both the friction and thrust ripple are considered and compensated by a linear friction model and B-spline wavelet neural networks, respectively. The experimental results not only verified the theoretical results in Section III, but also showed that the proposed method is superior to the existing methods. Future research will focus on the integrated design of the optimization of feed speed and control algorithm, which may improve the coordination and control precision of the system further.

References

[1] Z. Wang, C. Hu, and Y. Zhu, "Accelerated iteration algorithm based contouring error estimation for multi-axis motion control," *IEEE/ASME Trans. Mechatronics*, vol. 27, no. 1, pp. 452–462, Feb. 2022.

[2] Z. Wang, C. Hu, Y. Zhu, and L. Zhu, "Prediction-model-based contouring error iterative precompensation scheme for precision multiaxis motion systems," *IEEE/ASME Trans. Mechatronics*, vol. 26, no. 5, pp. 2274–2284, Oct. 2021.

[3] M. Tomizuka, "Zero phase error tracking algorithm for digital control," *J. Dyn. Syst. Meas. Control*, vol. 109, pp. 65–68, 1987.

[4] L. Lu, Z. Chen, B. Yao, and Q. Wang, "Desired compensation adaptive robust control of a linear-motor-driven precision industrial gantry with improved cogging force compensation," *IEEE/ASME Trans. Mechatronics*, vol. 13, no. 6, pp. 617–624, Dec. 2008.

[5] C. Hu, B. Yao, Z. Chen, and Q. Wang, "Adaptive robust repetitive control of an industrial biaxial precision gantry for contouring tasks," *IEEE Trans. Control Syst. Technol.*, vol. 19, no. 6, pp. 1559–1568, Nov. 2011.

[6] A. Safa, R. Y. Abdolmalaki, and H. C. Nejad, "Precise position tracking control with an improved transient performance for a linear piezoelectric ceramic motor," *IEEE Trans. Ind. Electron.*, vol. 66, no. 4, pp. 3008–3018, Apr. 2019.

[7] F. J. Lin and P. H. Chou, "Adaptive control of two-axis motion control system using interval type-2 fuzzy neural network," *IEEE Trans. Ind. Electron.*, vol. 56, no. 1, pp. 178–193, Jan. 2009.

[8] Z. Wang, C. Hu, Y. Zhu, S. He, K. Yang, and M. Zhang, "Neural network learning adaptive robust control of an industrial linear motor-driven stage with disturbance rejection ability," *IEEE Trans. Ind. Inform.*, vol. 13, no. 5, pp. 2172–2183, Oct. 2017.

[9] Y. Liu, W. Sun, and H. Gao, "High precision robust control for periodic tasks of linear motor via B-spline wavelet neural network observer," *IEEE Trans. Ind. Electron.*, vol. 69, no. 8, pp. 8255–8263, Aug. 2022.

[10] P. Sarachik and J. Ragazzini, "A 2-dimensional feedback control system," *Trans. Amer. Inst. Elect. Eng. Part II Appl. Ind.*, vol. 76, pp. 55–61, 1957.

[11] Y. Koren, "Cross-coupled biaxial computer control for manufacturing systems," *J. Dyn. Syst. Meas. Control*, vol. 102, pp. 265–272, 1980.

[12] S.-S. Yeh and P.-L. Hsu, "Analysis and design of the integrated controller for precise motion systems," *IEEE Trans. Control Syst. Technol.*, vol. 7, no. 6, pp. 706–717, Nov. 1999.

[13] Y. S. Tarng, H. Y. Chuang, and W. T. Hsu, "Intelligent cross-coupled fuzzy feedrate controller design for CNC machine tools based on genetic algorithms," *Int. J. Mach. Tools Manufacture*, vol. 39, pp. 1673–1692, 1999.

[14] S.-S. Yeh and P.-L. Hsu, "Estimation of the contouring error vector for the cross-coupled control design," *IEEE/ASME Trans. Mechatronics*, vol. 7, no. 1, pp. 44–51, Mar. 2002.

[15] B. Yao, S. Chan, and D. Wang, "Unified formulation of variable structure control schemes for robot manipulators," *IEEE Trans. Autom. Control*, vol. 39, vol. 2, pp. 371–376, Feb. 1994.

[16] B. Yao, C. Hu, and Q. Wang, "An orthogonal global task coordinate frame for contouring control of biaxial systems," *IEEE/ASME Trans. Mechatronics*, vol. 17, no. 4, pp. 622–634, Aug. 2012.

[17] R. D. Lorenz and P. B. Schmidt, "Synchronized motion control for process automation," in *Proc. Ind. Appl. Soc. Annu. Meeting*, 1989, pp. 1693–1698.

[18] R. Nakashima, S. Hao, H. Honda, R. Oguro, H. Miyakawa, and T. Tsuji, "Position control for a linear slider with twin linear drives," *Elect. Eng. Jpn. English Transl. Denki Gakkai Ronbunshi*, vol. 147, pp. 68–76, 2004.

[19] Perez-Pinal, C. Nunez, R. Alvarez, and I. Cervantes, "Comparison of multi-motor synchronization techniques," in *Proc. IEEE 30th Annu. Conf. Ind. Electron. Soc.*, vol. 2, 2004, pp. 1670–1675, doi: 10.1109/IECON.2004.1431832.

[20] S. M. Wang, R. J. Wang, and S. Tsooj, "A new synchronous error control method for CNC machine tools with dual-driving systems," *Int. J. Precis. Eng. Manuf.*, vol. 14, pp. 1415–1419, 2013.

[21] M. C. Tsai and B. H. Shen, "Synchronisation control of parallel dual inverted pendulums driven by linear servomotors," *IET Control Theory Appl.*, vol. 1, pp. 320–327, 2007.

[22] Y. Xiao and K. Y. Zhu, "Optimal synchronization control of high-precision motion systems," *IEEE Trans. Ind. Electron.*, vol. 53, no. 4, pp. 1160–1169, Jun. 2006.

[23] G. Zhong, Z. Shao, H. Deng, and J. Ren, "Precise position synchronous control for multi-axis servo systems," *IEEE Trans. Ind. Electron.*, vol. 64, no. 5, pp. 3707–3717, May 2017.

[24] C. Li, Z. Chen, and B. Yao, "Adaptive robust synchronization control of a dual-linear-motor-driven gantry with rotational dynamics and accurate online parameter estimation," *IEEE Trans. Ind. Inform.*, vol. 14, no. 7, pp. 3013–3022, Jul. 2018.

[25] G. Zhong, H. Yi, and W. Dou, "Design of dual-drive vertical lift servo system and synchronous control performance analysis," *IEEE/ASME Trans. Mechatronics*, vol. 25, no. 6, pp. 2927–2937, Dec. 2020.

[26] S. Yao, G. Gao, Z. Gao, and S. Li, "Active disturbance rejection synchronization control for parallel electro-coating conveyor," *ISA Trans.*, vol. 101, pp. 327–334, 2020.

[27] Z. Chen, C. Li, B. Yao, M. Yuan, and C. Yang, "Integrated coordinated/synchronized contouring control of a dual-linear-motor-driven gantry," *IEEE Trans. Ind. Electron.*, vol. 67, no. 5, pp. 3944–3954, May 2020.

[28] K. E. Atkinson and W. Han, *Theoretical Numerical Analysis—A Functional Analysis Framework*. Berlin, Germany: Springer, 2010.

[29] I. Daubechies. *Ten Lectures on Wavelets*. Philadelphia, PA, USA: SIAM, 1992.

[30] V. M. Matrosov, "Principle of comparison with Lyapunov vector function, Part I, IV," *Differ. Equ.*, vol. 5, no. 12, pp. 2129–2143, 1969.

Yanbin Liu received the B.S. degree in mathematics and the Ph.D. degree in control science and engineering from the Harbin Institute of Technology, Harbin, China, in 2012 and 2022, respectively.

He is currently a Postdoctoral Researcher with the Research Institute of Intelligent Control and Systems, Harbin Institute of Technology. His research interests focus on adaptive robust control and mechatronics.

Weichao Sun (Senior Member, IEEE) received the B.S. degree in automation from Central South University, Changsha, China, in 2007, the M.S. and Ph.D. degrees in control science and engineering from the Harbin Institute of Technology, Harbin, China, in 2009 and 2013, respectively.

He is currently a Professor with the Research Institute of Intelligent Control Systems, Harbin Institute of Technology. His research interests include adaptive robust control, mechatronics, robotics and autonomous vehicles.

Dr. Sun is an Associate Editor for IEEE TRANSACTIONS SYSTEMS, MAN, AND CYBERNETICS: SYSTEMS, MECHATRONICS and *Journal of Dynamic Systems, Measurement and Control*.

Concettina Buccella (Senior Member, IEEE) received the M.Sc. degree in electrotechnics from the University of L'Aquila, L'Aquila, Italy, in 1988, and the Ph.D. degree in electrical engineering from the University of Rome, "La Sapienza," Italy, in 1995.

From 1988 to 1989, she was a R&D Engineer with Italtel SpA, Italy. In 1991, she joined the University of L'Aquila, where she is a Professor of Power Converters, Electric Machines, and Drives with the Department of Information Engineering, Computer Science and Mathematics and the Chair of the B.Sc. degree in ICT Engineering. She is the Chief Scientific Officer with DigiPower srl, L'Aquila, Italy, an R&D company active in the field of power electronics. Her research interests include smart grids, power converters modulation techniques, renewable energy management, modeling of electrical and electronics systems, electromagnetic compatibility.

Prof. Buccella was the co-recipient of the 2012 and the 2013 Best Paper Award for the IEEE TRANSACTIONS ON INDUSTRIAL INFORMATICS. From 2014 to 2021, she has been an Associate Editor for the IEEE TRANSACTIONS ON INDUSTRIAL ELECTRONICS, and, since 2019, she is an Associate Editor for the IEEE SYSTEMS JOURNAL. She has been the Chair of the IEEE-IES Renewable Energy Systems Technical Committee, from 2017 to 2018.

Carlo Cecati (Fellow, IEEE) received the Dr. Ing. degree in electrotechnical engineering from the University of L'Aquila, L'Aquila, Italy, in 1983.

He has been a Professor with the University of L'Aquila, since 2006, and Rector's delegate, from 2005 to 2013. From September 2015 to September 2017, he was a Qianren Talents Professor with the Harbin Institute of Technology, Harbin, China. He has authored more than 250 journal and conference papers in the areas of his interests. His research interests include power electronics, distributed generation, smart grids, and e-transportation.

Prof. Cecati was the recipient of the 2017 Antony J. Hornfeck Award and the 2021 Dr.-Ing. Eugene Mittelmann Achievement Award, both from the IEEE Industrial Electronics Society. He was the co-recipient of the 2012 and of the 2013 Best Paper Award from the IEEE TRANSACTIONS ON INDUSTRIAL INFORMATICS, of the 2012 Best Paper Award from the IEEE INDUSTRIAL ELECTRONICS MAGAZINE, and of the 2019 Outstanding Paper Award from the IEEE TRANSACTIONS ON INDUSTRIAL ELECTRONICS.